BIOCHEMISTRY
including biophysical chemistry & molecular biology
Article

Biochemistry **2009,** *48,* 7939–7947 7939
DOI: 10.1021/bi900907a

Ternary Complexes of Iron, Amyloid-β, and Nitrilotriacetic Acid: Binding Affinities, Redox Properties, and Relevance to Iron-Induced Oxidative Stress in Alzheimer's Disease[†]

Dianlu Jiang,[‡] Xiangjun Li,[‡] Renee Williams,[‡,§] Sveti Patel,[‡] Lijie Men,[§] Yinsheng Wang,[§] and Feimeng Zhou*[,‡]

[‡]*Department of Chemistry and Biochemistry, California State University, Los Angeles, California 90032, and* [§]*Department of Chemistry, University of California, Riverside, California 92951*

Received May 28, 2009; Revised Manuscript Received July 9, 2009

ABSTRACT: The interaction of amyloid-β (Aβ) and redox-active metals, two important biomarkers present in the senile plaques of Alzheimer's disease (AD) brain, has been suggested to enhance the Aβ aggregation or facilitate the generation of reactive oxygen species (ROS). This study investigates the nature of the interaction between the metal-binding domain of Aβ, viz., Aβ(1−16), and the Fe(III) or Fe(II) complex with nitrilotriacetic acid (NTA). Using electrospray ionization mass spectrometry (ESI-MS), the formation of a ternary complex of Aβ(1−16), Fe(III), and NTA with a stoichiometry of 1:1:1 was identified. MS also revealed that the NTA moiety can be detached via collision-induced dissociation. The cumulative dissociation constants of both Aβ−Fe(III)−NTA and Aβ−Fe(II)−NTA complexes were deduced to be 6.3×10^{-21} and 5.0×10^{-12} M^2, respectively, via measurement of the fluorescence quenching of the sole tyrosine residue on Aβ upon formation of the complex. The redox properties of these two complexes were investigated by cyclic voltammetry. The redox potential of the Aβ−Fe(III)−NTA complex was found to be 0.03 V versus Ag/AgCl, which is negatively shifted by 0.54 V when compared to the redox potential of free Fe(III)/Fe(II). Despite such a large potential modulation, the redox potential of the Aβ−Fe(III)−NTA complex is still sufficiently high for a range of redox reactions with cellular species to occur. The Aβ−Fe(II)−NTA complex electrogenerated from the Aβ−Fe(III)−NTA complex was also found to catalyze the reduction of oxygen to produce H_2O_2. These findings provide significant insight into the role of iron and Aβ in the development of AD. The binding of iron by Aβ modulates the redox potential to a level at which its redox cycling occurs. In the presence of a biological reductant (antioxidant), redox cycling of iron could disrupt the redox balance within the cellular milieu. As a consequence, not only is ROS continuously produced, but oxygen and biological reductants can also be depleted. A cascade of biological processes can therefore be affected. In addition, the strong binding affinity of Aβ toward Fe(III) and Fe(II) indicates Aβ could compete for iron against other iron-containing proteins. In particular, its strong affinity for Fe(II), which is 8 orders of magnitude stronger than that of transferrin, would greatly interfere with iron homeostasis.

A major hallmark of Alzheimer's disease (AD)[1] is the deposition of aggregates of amyloid-β (Aβ) peptides in the senile plaques (*1*). The in vivo aggregation/deposition of Aβ peptides is suggested to enhance neurotoxicity or be a result of aberrant cellular processes (*2*). The amyloid cascade hypothesis has also been closely interwoven with its counterpart of oxidative stress (*2*, *3*). A major form of oxidative stress is caused by reactive oxygen species (ROS) whose generation might be facilitated by redox-active metal ions such as Cu(II), Fe(III), and Fe(II). The fact that in the senile plaques high levels of these metal ions exist [e.g., Cu(II) at ~0.4 mM and Fe(III) at ~0.9 mM] (*4*) supports this contention. Deleterious effects associated with ROS have been linked to extensive oxidative damage to proteins (*5*) and DNA (*6*−*8*), decreased levels of polyunsaturated fatty acids (*9*), increased levels of lipid peroxidation (*3*, *10*), and mitochondrial dysfunction (*11*, *12*).

On the basis that both Aβ peptides and redox-active metals are concentrated in senile plaques, intensive research efforts have focused on the formation, identification, and characterization of such Aβ−metal complexes (*13*−*16*). It is shown that the hydrophilic domain (residues 1−16) of the full-length Aβ can ligate Cu(II) through its histidine and possibly glutamate, aspartate, and/or tyrosine residues (*4*, *14*, *17*, *18*). A Raman analysis of postmortem brain samples has also confirmed the existence of the Aβ−Cu complex in senile plaques (*19*). Although it is known that Aβ peptides are segments truncated from the amyloid protein precursor or APP [e.g., Aβ(1−16) is cleaved by α- and β-secretases in vivo (*20*)], the exact biological functions of Aβ peptides and APP are still not clear. Given that structurally the copper-binding domain of APP is similar to Cu chaperones and that Cu can modulate Aβ and APP cellular levels (*21*), APP has been presumed to partake in intracellular copper homeostasis.

[†]This work is supported by National Institutes of Health Grants GM 08101 to F.Z. and R01 CA 101864 and R01 CA 116522 to Y.W. and partially supported by the NIH-RIMI Program at California State University—Los Angeles (CSULA, P20 MD001824-01 to F.Z.) and the NSF-LSAMP Program at CSULA (HRD 0331537 to R.W.). X.L. thanks the Chinese Academy of Sciences for financial support.

*To whom correspondence should be addressed. Phone: (323) 343-2390. Fax: (323) 343-6490. E-mail: fzhou@calstatela.edu.

[1]Abbreviations: AD, Alzheimer's disease; Aβ, β-amyloid; NTA, nitrilotriacetic acid; APP, amyloid precursor protein; ROS, reactive oxygen species; ET, electron transfer; Met-35, methionine at position 35; Tyr-10, tyrosine at position 10; Asp-1, aspartic acid at position 1; Glu-3, glutamic acid at position 3; His-6, histidine at position 6; Asp-7, aspartic acid at position 1; Glu-11, glutamic acid at position 11; His-13, histidine at position 13; His-14, histidine at position 14; CV, cyclic voltammetry; ESI-MS, electrospray ionization mass spectrometry; HEPES, 4-(2-hydroxyethyl)-1-piperazineethanesulfonic acid.

Published on Web 07/14/2009

Overexpression of APP results in Cu deficiency and consequently reduces the activity of superoxide dismutase (SOD-1) (*22*), a key enzyme in scavenging reactive oxygen radicals. In vitro studies have shown that incubation of an Aβ/Cu(II) mixture with electron donors (e.g., ascorbic acid) under aerobic conditions produces H_2O_2 (*23*, *24*). Recently, we successfully measured the redox potential of the Aβ−Cu(II) complex using voltammetric techniques. We and others also confirmed that H_2O_2 production can indeed occur via the Aβ−Cu(I) complex-catalyzed reduction of oxygen (*24*, *25*). The amount of H_2O_2 is greatest in the presence of the electroreduced Aβ(1−16)−Cu(I) complex [i.e., Aβ(1−16)−Cu(I)] (*25*).

Similar to copper, iron is essential to a variety of brain functions. Iron in brain is highly regulated by proteins such as ferritin and transferrin (*26*). The iron load increases with age and becomes acutely high in AD patients (*27*, *28*). It was found that postmortem tissues from AD brains accelerate production of ROS in vitro when a reductant is present, and the iron chelator deferroxamine appears to decelerate ROS production (*29*). Smith et al., through speciation of Fe(II) and Fe(III) in hippocampal tissues from several AD patients, have shown that iron that has accumulated in senile plaques can lead to generation of free radicals (*30*). Thus, it is conceivable why little free and reactive forms of iron are present in normal brain and translocation of iron must be chaperoned (*31*). Small inorganic and organic ligands are also important in transfixing and modulating the transfer of iron in and between various metalloenzymes (*32*). For example, the bicarbonate anion in transferrin renders Fe(III) in a tight coordination sphere and is partially responsible for its high affinity for Fe(III) (ca. 10^{-19}−10^{-20} M) (*33*). Phosphate, carboxylates, and peptides serve as ligands for iron in the so-called "labile iron pool" (*21*, *34*). However, to the best of our knowledge, no in vivo studies have unequivocally demonstrated that iron is complexed by Aβ in the senile plaque. Moreover, because of the rapid hydrolysis of Fe(III), in vitro formation of the putative Aβ−Fe(III) complex via simple mixing of Fe(III) and Aβ has been largely unsuccessful and is qualitative at best. Without quantitative formation of Fe-containing Aβ complexes in vitro and knowledge of their redox potentials, the hypothesis that ROS are concertedly produced by Aβ and iron remains speculative. Considering that free Fe(III) is an even stronger oxidant than free Cu(II), the paucity of information about any Fe-containing Aβ complexes heightens the need to understand the relative contribution to oxidative stress in AD between iron and copper. Moreover, measuring the binding affinity of Aβ for an Fe(III)-containing species with respect to that toward the Fe(II) variant should also provide insight into the relative stability of the complexes when the iron centers are reduced.

We report, for the first time, the formation of a ternary complex containing Aβ(1−16), Fe(III), and nitrilotriacetic acid (NTA). The use of a preformed Fe(III)−NTA complex as the Fe(III) source for producing this ternary complex prevents the hydrolysis of free Fe(III) at physiological pH. The Fe(III)−NTA complex has long been used as a supply of Fe(III) for various biological studies (*35*). Furthermore, the moderate binding affinity of NTA for iron (1.3×10^{-16} M) (*36*) makes it an excellent mimetic of small ligands involved in metal−chaperone proteins. Electrospray ionization mass spectrometry (ESI-MS) was used to determine the binding stoichiometry among Aβ(1−16), Fe(III), and NTA, and MS^n conducted in an ion trap allowed us to assess the relative binding strength between Aβ and NTA toward the iron center and the potential binding sites of Aβ. MS analysis of the isotopic peaks of the complex helped pinpoint the oxidation state of the iron center upon formation of the complex. The cumulative dissociation constants of both the Aβ−Fe(III)−NTA and Aβ−Fe(II)−NTA complexes were deduced by monitoring the quenching of the fluorescence of the sole tyrosine residue of Aβ during formation of the complex. As in our previous approach in interrogating the H_2O_2 generation facilitated by the electrogenerated Aβ complex of Cu(I), the Aβ−Fe(II)−NTA complex was found to catalyze the reduction of oxygen to H_2O_2. The roles of Fe(III) and Fe(II) in participating in ROS generation and redox reactions with representative cellular species are discussed in the context of oxidative stress in AD.

MATERIALS AND METHODS

Materials. Lyophilized Aβ(1−16) (DAEFRHDSGYEVHHQK, denoted Aβ in the study) samples were either purchased from rPeptide (Bogart, GA) or synthesized and purified in house. Other chemicals were of analytical grade (Sigma-Aldrich). All the aqueous solutions were prepared using deionized water (Millipore, 18 MΩ cm). Throughout the work, 10 mM $FeCl_3$ dissolved in 20 mM nitrilotriacetic acid (NTA) was used as the Fe(III) stock solution. We prepared fresh Aβ(1−16) solutions by dissolving lyophilized Aβ samples in deionized water. For the experiment with Fe(II), $FeSO_4 \cdot 7H_2O$ (10 mM) was dissolved in a 20 mM NTA solution. To avoid the Fe(II) oxidation by oxygen, samples were prepared in a glovebox constantly flushed with N_2 with aqueous solutions thoroughly purged with N_2.

Mass Spectrometry. The mass spectra were recorded on a LTQ linear ion trap mass spectrometer (Thermo Electron, San Jose, CA) equipped with an electrospray ionization (ESI) source. Aβ was first dissolved in a water/methanol solution (50:50, v/v) to yield a 50 μM Aβ stock solution. The Aβ solution and an aliquot spiked with 50 μM Fe(III)−NTA complex were separately analyzed.

Electrochemical Measurements. Electrochemical experiments were performed on a CHI 832 electrochemical workstation (CH Instruments, Austin, TX) using a homemade plastic electrochemical cell. A glassy carbon disk electrode and a platinum wire were used as the working and counter electrodes, respectively. All the potential values are reported with respect to the Ag/AgCl reference electrode. Prior to each experiment, the glassy carbon electrode was polished with diamond pastes 15 and 3 μm in diameter and alumina pastes 1 and 0.3 μm in diameter (Buehler, Lake Bluff, IL). The electrolyte solution was a 20 mM acetate/20 mM 4-(2-hydroxyethyl)-1-piperazineethanesulfonic acid (HEPES) buffer (pH 7.0) containing 0.1 M $NaNO_3$. Aliquots of Aβ from stock solutions were diluted with the acetate buffer to the desired concentrations. For voltammetric studies, these Aβ solutions were spiked with Fe(III)−NTA or Fe(II) − NTA stock solution to predefined Aβ:iron molar ratios.

Spectrofluorometric Measurements. Steady-state fluorescence measurements of the tyrosine residue at position 10 in Aβ were conducted at room temperature using a Cary Eclipse spectrofluorometer (Varian Inc., Palo Alto, CA). The procedure follows our earlier work on the measurement of the binding constants of the Aβ−Cu(II) complexes (*37*). On the basis of the aforementioned MS studies, it can be assumed that the change in fluorescence upon addition of the Fe(III)−NTA complex to the Aβ(1−16) solution reflects the amount of ternary complex produced. The dissociation constant (K_{d1}) was determined from

the plot of fluorescence intensity versus the total Fe(III)−NTA complex concentration, [L], using the following equation:

$$\Delta F = F_0 - F_L = \frac{F_0 - F_\alpha}{2[M_0]}\{[L]+[M_0]+K_{d1} - [([L]+[M_0]+K_{d1})^2 - 4[M_0][L]]^{1/2}\} \quad (1)$$

where F_0 and F_L are the measured fluorescence intensities of Aβ(1−16) at 303 nm in the absence and presence of the Fe(III)−NTA complex, respectively, F_α is the intensity of the solution in which the Aβ fluorescence is completely quenched by the Fe(III)−NTA complex, and $[M_0]$ is the Aβ concentration which was varied in the range of 10−100 μM for the fitting procedure. Equation 1 holds when the concentration of metal binding sites exceeds the dissociation constant of the complex. For Aβ binding with the Fe(II)−NTA complex, the experiment was again conducted in the glovebox continuously circulated with N_2. The fluorescence measurement was performed with the cuvette containing the complex solution sealed inside the glovebox.

Detection of Hydrogen Peroxide. The electrode potential was held at −0.05 V to reduce the Aβ−Fe(III)−NTA complex. H_2O_2 generated was monitored using the Fluoro H_2O_2 detection kit (Cell Technology Inc., Mountain View, CA), which was also utilized in our previous studies of Aβ−Cu(I) complex-catalyzed H_2O_2 generation (*25*). In the presence of H_2O_2 and horseradish peroxidase (HRP), 10-acetyl-3,7-dihydroxyphenoxazine (ADHP) is rapidly oxidized to a fluorescent product, resorufin. The procedure involved adding 50 μL of the sample solution to a 50 μL aliquot of the reaction cocktail, which contained 100 μL of 10 mM ADHP, 200 μL of 10 units/mL HRP, and 4.7 mL of reaction buffer. The mixture was then incubated at room temperature in the dark for 10 min. Subsequently, the fluorescence intensity of resorufin was measured at an excitation wavelength of 550 nm. Via comparison of the fluorescence intensity of resorufin in the sample solution to that of the control, the amount of H_2O_2 can be measured.

RESULTS

Fe(III) Retains Its Oxidation State in Its Complex with Aβ. We have demonstrated previously that high-resolution MS is a viable technique for determining both the oxidation state and the binding stoichiometry of the Aβ−Cu(II) complex (*25*). The identification of the oxidation state of the metal center in the metal complex of Aβ is of particular interest, since the relevant biological redox reactions are largely dictated by the metal center [i.e., Cu(II) vs Cu(I) or Fe(III) vs Fe(II)] (*38*). Moreover, tyrosine (Tyr-10) and methione (Met-35) are oxidizable, and many studies have focused on the possible redox reactions between them and the metal center(s) (*39*−*41*). The oxidation potential of Met-35 is much higher than that of Tyr-10 (*42*). We and others have recently shown that the Tyr-10 residue remains intact when Cu(II) forms a complex with Aβ and concluded that Cu complexation does not chemically modify any Aβ residues (*25*).

Figure 1 shows a mass spectrum collected from a mixture of Aβ(1−16) and the Fe(III)−NTA complex. The predominate peaks are of the +2, +3, and +4 charge states. The peaks clustered around m/z 489.82 and 550.82 correspond to quadruply charged Aβ(1−16) Aβ(1−16)−Fe−NTA complex, respectively. The intense peak at m/z 489.82 is consistent with our previous positive-ion ESI-MS of Aβ(1−16) alone (*25*). Increasing the

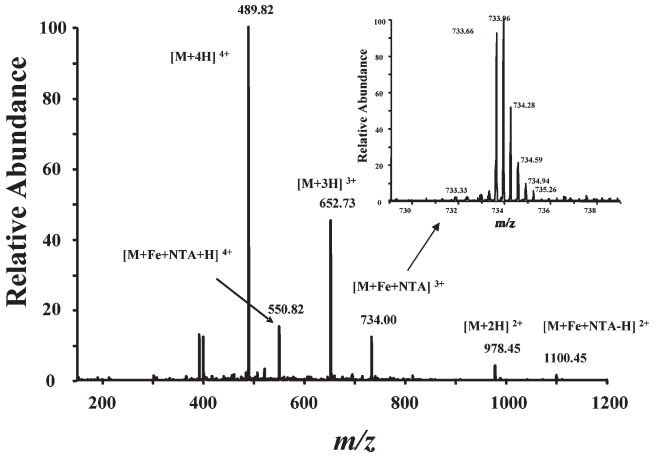

FIGURE 1: Positive-ion ESI-MS of Aβ(1−16) and the Fe(III)−NTA complex mixed at a 1:1 molar ratio. The inset shows the MS of the triply charged Aβ(1−16)−Fe(III)−NTA complex collected from a high-resolution ultrazoom scan.

molar ratio of the Fe(III)−NTA complex and Aβ in the mixture only changed the relative abundances of ions corresponding to free Aβ and the complex and did not generate peaks indicative of other binding stoichiometries. Therefore, our ESI-MS indicates that an Aβ−Fe−NTA ternary complex has formed. The absence of an Aβ−Fe(III) binary complex peak in Figure 1 suggests that, even if present, it would not be a predominant species in solution. When ferric ion was added directly into an Aβ solution, no mass peaks corresponding to an Fe-containing Aβ complex were detected. This is expected since hydrolysis of Fe(III) at neutral pH is rapid and predominant (*43*). The use of NTA inhibits the hydrolysis of Fe(III), allowing Aβ to bind to the Fe(III)−NTA complex.

Previously, by comparing the experimentally measured isotopic peak profiles of various Aβ−Cu complexes to theoretical values corresponding to the two different Cu oxidation states (+2 vs +1), we unambiguously concluded that Cu(II) retains its oxidation state in the complexed form (*25*). The oxidation state of the iron center in the Aβ−Fe(III)−NTA ternary complex can be deduced similarly. Table S1 of the Supporting Information lists the experimentally determined isotopic peaks of the triply and quadruply charged species to the theoretical m/z values of the Aβ−Fe(III)−NTA and Aβ−Fe(II)−NTA complexes. If Fe(II) were produced during formation of the complex, the complex would be doubly protonated to yield a +4 ion; on the other hand, if the iron center had an oxidation state of +3, the complex would need to be only singly protonated to reach a charge state of +4. The deviations for the triply charged ions between the measured and calculated m/z values of the Aβ−Fe(III)−NTA complex are markedly smaller than those of the hypothetical Aβ−Fe(II)−NTA complex. This indicates that the iron center has the same oxidation state as that in the Fe(III)−NTA complex. The analysis of the isotopic peaks for the +4 ions led to the same conclusion (Table S1 of the Supporting Information). A mass spectrum of the complex collected in the high-resolution ultrazoom scan mode is shown in the inset of Figure 1.

Since the oxidation state of Fe(III) remains unchanged, the Aβ−Fe(III)−NTA complex must be incapable of oxidizing Tyr-10 to the semiquinone product. This conclusion is also confirmed by our voltammetric experiment (vide infra). Therefore, Met-35 in the full-length Aβ should not be oxidized, because, as aforementioned, methionine has an oxidation potential much higher

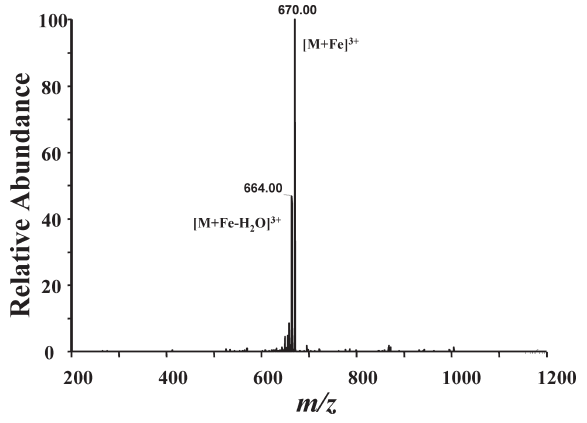

FIGURE 2: Product ion spectrum of the triply charged ion of the Aβ(1−16)−Fe(III)−NTA complex (m/z 733.9).

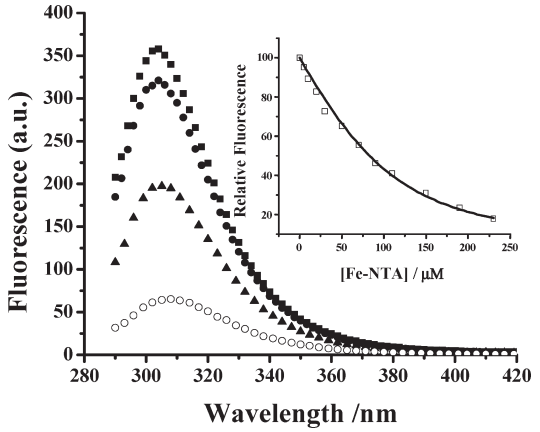

FIGURE 3: Fluorescence spectra of 100 μM Aβ(1−16) in 0.02 M HEPES buffer (pH 7.00) (■) and 100 μM Aβ(1−16) solutions that contained 10 (●), 70 (▲), and 210 μM Fe(III)−NTA complex (○). The inset shows the determination of K_{d1} using the tyrosine fluorescence quenched by the Fe(III)−NTA complex. The white squares are experimental data, and the curve is the fit using eq 1 with a K_{d1} of 3.2×10^{-5} M ($r^2 = 0.999$).

than that of tyrosine (*42*). The oxidation potential for the free Fe(III)/Fe(II) couple is 0.57 V versus Ag/AgCl (*44*), which is close to that of tyrosine (irreversible oxidation peak between 0.60 and 0.75 V) and substantially more positive than those of both the free Cu(II)/Cu(I) (−0.041 V vs Ag/AgCl) and Cu(II)/Cu(0) (0.148 V vs Ag/AgCl) couples (*45*). Apparently, the formation of a ternary metal complex has attenuated the relatively high oxidation potential of free Fe(III) to a low value at which Tyr-10 cannot be oxidized.

We also conducted MS/MS studies of the ternary complex and found that the NTA moiety can be readily eliminated from the complex upon collision-induced dissociation in the gas phase (Figure 2). In fact, triply charged ions corresponding to the Aβ−Fe(III) complex (m/z 670.00) or its dehydrated form (m/z 664.00) dominate the product ion spectrum, suggesting that Aβ is a multidentate ligand that may bind Fe(III) more strongly than NTA. Therefore, although Aβ may not completely replace NTA in the coordination sphere, rearrangement of the binding sites and partial replacement of NTA sites by Aβ could occur in both solution and gas phases. Further tandem MS analysis of the fragments arising from cleavage of the daughter ion of m/z 670 revealed the facile formation of $[b_{13} + Fe]$, $[b_{14} + Fe]$, $[b_{15} + Fe]$, and $[y_{15} + Fe]$ ions as well as their dehydrated counterparts, though y_2, y_8, y_9, and b_7 ions are also produced in lower abundance (Figure S1a of the Supporting Information). In contrast, the product ion spectrum of the $[M + 3H]^{3+}$ ion of the uncomplexed Aβ revealed extensive cleavage along the entire peptide backbone (Figure S1b of the Supporting Information). The absence of abundant fragment ions emanating from the cleavage of the middle portion of the peptide might be attributed to the coordination of Fe(III) with multiple residues in this peptide segment. In this regard, the facile cleavages leading to the formation of abundant $[b_{13} + Fe]$, $[b_{14} + Fe]$, $[b_{15} + Fe]$, and $[y_{15} + Fe]$ ions indicate that the N-terminal aspartic acid residue and the three residues located close to the C-terminus of the peptide might not be substantially involved in Fe(III) binding. The identification of exact binding sites requires more investigation. However, histidines and carboxylic groups of aspartic and glutamic residues are possible binding sites. In particular, histidines have been demonstrated to be involved in binding irons in postmodem senile plaque tissues of AD brain (*30*).

Determination of Binding Affinity. We (*37*) and others (*14*, *46*) have shown that the Tyr-10 fluorescence is sensitive to structural changes caused by complexation of Cu(II) to the hydrophilic domain of Aβ. The fluorescence peak at 303 nm for Aβ in the presence of the Fe(III)−NTA complex was therefore used to estimate the dissociation constant, K_{d1}, of the Aβ−Fe(III)−NTA complex. The variation of Aβ fluorescence intensity as a function of the Fe(III)−NTA complex concentration (Figure 3) was analyzed by means of a nonlinear least-squares regression using eq 1. The observed dissociation constant is 3.2×10^{-5} M, which is ~1 order of magnitude larger than that between the C-lobe of transferrin and the Fe−NTA complex (*47*). Therefore, we conclude that the binding between Aβ and the Fe−NTA complex is quite strong. This is consistent with the above-mentioned MS that displays intense complex peaks.

When NTA is in excess, two possible complexes between Fe(III) and NTA, viz., Fe(III)−NTA and Fe(III)−NTA_2, could exist. Thus, depending on the relative abundance of the two Fe−NTA species, one of the following two equilibria will be predominant:

$$A\beta + Fe(III)-NTA \leftrightarrow A\beta-Fe(III)-NTA \quad (2)$$

$$A\beta + Fe(III)-NTA_2 \leftrightarrow A\beta-Fe(III)-NTA + NTA \quad (3)$$

For the sake of simplicity, the charges of the ions involved in the Aβ−iron equilibria have been omitted. In eq 3, the binding of Aβ to the Fe(III)−NTA_2 complex competes out an NTA ligand. If such a competition were at work, then the measured binding constant would be dependent on the concentration of NTA. To pinpoint the equilibrium responsible for the observed Aβ−Fe(III)−NTA ternary complex, we measured the K values at various initial NTA concentrations. We also conducted the same measurements using the Fe(II)−NTA complex. The results are compiled in Table 1.

The fact that the K_{d1} values are not significantly dependent on the NTA concentration indicates that eq 3 is not important. This may be explained by the weaker ligation involving the second NTA group (*36*).

The dissociation constant for eq 2 can be expressed by

$$K_{d1} = \frac{[A\beta][Fe(III)-NTA]}{[A\beta-Fe(III)-NTA]} \quad (4)$$

Table 1: Apparent Dissociation Constants of Aβ−Fe(III)−NTA and Aβ−Fe(II)−NTA Complexes Measured at Different NTA Concentrations

	0.0 mM NTA[a]	1.0 mM NTA[a]	2.0 mM NTA[a]
K_{d1} (M) [Aβ−Fe(III)−NTA]	$(3.2 \pm 0.1) \times 10^{-5}$	$(5.5 \pm 0.4) \times 10^{-5}$	$(5.3 \pm 0.3) \times 10^{-5}$
K_{d1} (M) [Aβ−Fe(II)−NTA]	$(3.4 \pm 0.1) \times 10^{-4}$	$(4.2 \pm 0.3) \times 10^{-4}$	$(2.9 \pm 0.2) \times 10^{-4}$

[a] Initial concentration.

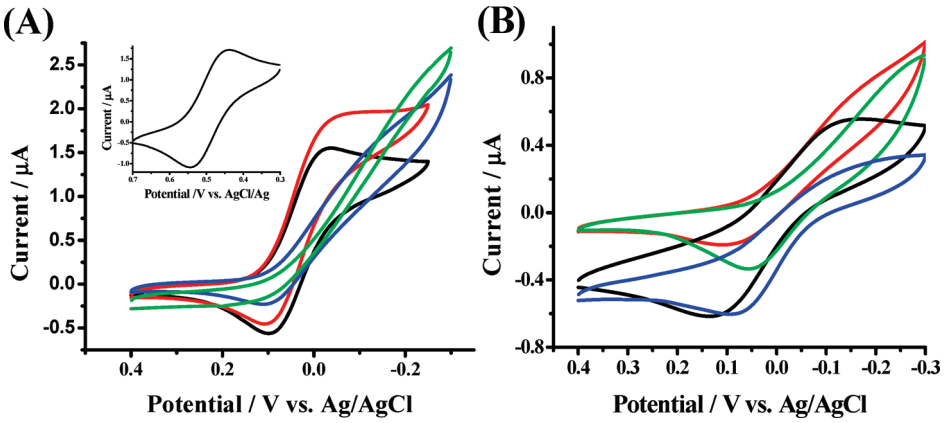

FIGURE 4: Cyclic voltammograms of (A) deaerated 400 μM Fe(III)−NTA complex in the presence (black) and absence (blue) of 1 mM Aβ(1−16) and (B) the same as panel A except that the Fe(III)−NTA complex was replaced with the Fe(II)−NTA complex at the same concentration. The red and green curves in both panels correspond to air-saturated solutions of the Fe(III)−NTA complex with and without Aβ(1−16), respectively. All solutions were prepared with a buffer containing 20 mM HEPES, 20 mM acetate, and 0.2 M $NaNO_3$ (pH 7.0). The inset in panel A depicts a CV of 1 mM $FeCl_3$ prepared in 1 M HCl and 1 M $CaCl_2$ and acquired at an electrochemically treated glassy carbon electrode. The scan rate used for all voltammograms was 2 mV/s.

The complexation equilibrium between Fe(III) and NTA can be written as follows:

$$\text{Fe(III)} + \text{NTA} = \text{Fe(III)}-\text{NTA} \quad (5)$$

and the corresponding dissociation constant is

$$K_{d2} = \frac{[\text{Fe(III)}][\text{NTA}]}{[\text{Fe(III)}-\text{NTA}]} \quad (6)$$

Therefore, the cumulative dissociation constant can be derived as

$$K_d = \frac{[\text{A}\beta][\text{Fe(III)}][\text{NTA}]}{[\text{A}\beta-\text{Fe(III)}-\text{NTA}]} = K_{d1}K_{d2} \quad (7)$$

The commonly accepted value for K_{d2} is 1.3×10^{-16} M (*36*), and the average value measured here for K_{d1} is 5.0×10^{-5} M. Thus, the cumulative dissociation constant (K_d) equals 6.3×10^{-21} M^2.

For the complexation of the Fe(II)−NTA complex with Aβ, the NTA concentration was also found to have little influence on K_{d1}. Equilibrium equations analogous to eqs 4 and 6 can be written for formation of the Aβ−Fe(II)−NTA complex. The dissociation constant of the Fe(II)−NTA complex has been reported to be 1.7×10^{-8} M (*36*). Therefore, the cumulative dissociation constant (K_d) of the Aβ−Fe(II)−NTA complex is estimated to be 5.0×10^{-12} M^2.

Redox Potentials of the Aβ−Fe(III)−NTA and Aβ−Fe(II)−NTA Complexes. Redox cycling of iron accompanied by production of ROS has long been considered to be responsible for the iron toxicity in biological systems (*48*). As mentioned earlier, little free Fe(III) or Fe(II) exists in an organism because most of these irons are either stored in the redox-inactive oxide forms or bound by siderophores (*21*). Sequestration of Fe(III) or Fe(II) by protein (peptide) shifts the redox potential of the Fe(III)/Fe(II) couple to much more negative values [the Fe(III) center is more difficult to reduce or its oxidizing power is decreased], making the metal centers inaccessible to redox-active biomolecules. Thus, depending on the iron coordination spheres and the relative binding affinities of proteins and peptides for Fe(III) or Fe(II), the redox potentials of the resultant iron complexes will vary. As a result, the extent of ROS production is greatly influenced by the Fe(II) and Fe(III) coordination chemistry. As mentioned in the introductory section, without knowledge of the redox potentials of the Aβ−Fe(III) or Aβ−Fe(II) complex, it has been difficult to interpret biological redox reactions that might be induced or modulated by the iron-containing Aβ complexes.

Figure 4A is an overlay of a series of cyclic voltammograms (CVs) recorded under different experimental conditions. CVs of Fe(III)−NTA alone and Aβ(1−16) in the presence of the Fe(III)−NTA complex are shown as blue and black curves, respectively. To examine the effect of oxygen on the redox behavior of the Aβ−Fe(III)−NTA complex, we also bubbled O_2 into and collected CVs from a mixture of Aβ(1−16) and the Fe(III)−NTA complex (red curve) and a Fe(III)−NTA solution (green curve). In the mixture of Aβ(1−16) and the Fe(III)−NTA complex, a pair of quasi-reversible waves was observed with an oxidation peak at 0.094 V and a reduction peak at ca. −0.034 V. The redox peaks can be assigned to the reduction and reoxidation of the Aβ−Fe(III)−NTA complex, and $E^\circ_{1/2}$ was therefore approximated to be 0.03 V. The redox behavior of the Aβ−Fe(III)−NTA complex is in contrast to the irreversible CV of the Fe(III)−NTA complex. We also obtained a CV of Fe(II) and found the $E^\circ_{1/2}$ value (0.50 V; see also the inset of Figure 4A) to be close to the theoretical value [0.57 V (*44*)]. The small deviation between our measured value and the theoretical values can be ascribed to the dependence of heterogeneous electron transfer rates on the pretreatment of the glassy carbon electrode surface (*49*). Comparison of the theoretical $E^\circ_{1/2}$ value of the Fe(III)/Fe(II) couple to that of the Aβ−Fe(III)−NTA/Aβ−Fe(II)−NTA complexes measured in this work shows a 0.54 V shift in

the cathodic (negative) direction upon Aβ complexation. Such a shift is in excellent agreement with the value (0.53 V) calculated on the basis of the cumulative stability constants of the Aβ−Fe(III)−NTA and Aβ−Fe(II)−NTA complexes (cf. Table 1). We note that the redox potential of the complex is much higher than those of representative iron-containing proteins or complexes, such as transferrin and iron siderophore complexes (*43*). In the presence of O_2, the magnitude of the reduction peak (red curve in Figure 4A) was found to increase at the expense of the oxidation peak, suggesting the catalytic nature of the reaction and the involvement of O_2.

The Aβ−Fe(II) Complex Catalyzes the Reduction of Oxygen to Hydrogen Peroxide. As mentioned above, the reduced form of the Aβ−Fe(III)−NTA complex can catalyze oxygen reduction, which could lead to the generation of either H_2O_2 or H_2O. To determine if the reduced complex can catalyze the reduction of oxygen to H_2O_2, we conducted spectrofluorometric detection of H_2O_2 from aliquots of an Aβ−Fe(III)−NTA solution that had been subjected to controlled-potential electrolyses.

After electrolyses of these solutions at −0.05 V for different amounts of time, the solutions were analyzed for the amount of H_2O_2 generated. We chose −0.05 V because the electrocatalytic reduction peak of the complex is close to the maximum value (plateau) but the reduction of any unbound Fe(III)−NTA complex is relatively small. As shown in Figure 4, for the mixture of Aβ and the Fe(III)−NTA complex, the magnitudes of the fluorescence peaks increase with electrolysis time and are significantly greater than those of the same mixture that had not been electrolyzed (black curve) and the Fe(III)−NTA complex only solution (magenta). It is worth mentioning that the fluorescence intensity measured from the Fe(III)−NTA solution electrolyzed for different times remained largely unchanged (data not shown), suggesting that the Fe(II)−NTA complex was not generated or the Fe(II)−NTA complex could react with O_2 via a different process [e.g., generation of superoxide radical (*24*)]. All these observations indicate that it is the reduced Aβ−Fe(III)−NTA complex that is responsible for the H_2O_2 production. In fact, the amount of H_2O_2 produced is greatest when the initial solution contains the Aβ−Fe(II)−NTA complex and O_2 (light blue curve in Figure 5).

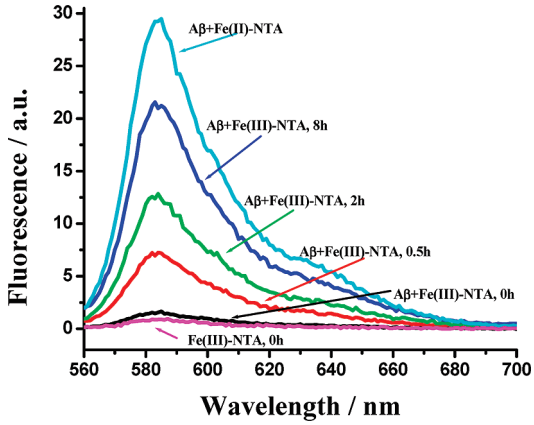

FIGURE 5: Fluorescence spectra of resorufin for detecting H_2O_2 in solutions of the Aβ−Fe(III)−NTA complex before (black) and after electrolyses for different amounts of time (red, green, and dark blue), the Aβ−Fe(II)−NTA complex (light blue), and the Fe(III)−NTA complex (purple). The times for electrolysis at −0.05 V are 0.5 (red), 2 (green), and 8 h (dark blue). The concentration of Aβ in all sample solutions was 1 mM, whereas those of the Fe(III)−NTA and Fe(II)−NTA complexes were 400 μM.

DISCUSSION

It is generally believed that the metal binding domain in Aβ is within the segment comprising residues 1−16, with Asp-1, Glu-3, His-6, Asp-7, Tyr-10, Glu-11, His-13, and His-14 as the possible binding sites (*50*, *51*). Our MS study has demonstrated that Aβ is capable of binding Fe(III) in the presence of NTA, forming a ternary complex with a 1:1:1 stoichiometry. Although the exact sites of binding to Fe(III) are not known, this represents the first study of an Fe(III)-containing Aβ complex. Our MS^3 data (see Figure S1 of the Supporting Information) suggest that Aβ possesses multiple binding sites toward Fe. In addition, nitrogen (especially that on the imidazole rings in the histidine residues) binds Fe(II) relatively stronger than oxygen in the carboxylic group, and consequently, the nitrogen-coordinated iron complex should have a more positive redox potential than the corresponding oxygen-coordinated counterpart. Comparing the CVs of the Fe−NTA and Aβ−Fe−NTA complexes, we found the potential actually was indeed shifted positively. This further suggests that nitrogen-containing groups (from histidines) bind iron. In vivo, the level of free Fe(III) ion is extremely low (on the order of 10^{-18} M) (*43*). The cumulative dissociation constant measured by us is on the order of 10^{-20} M^2, suggesting that the Fe(III) hydrolysis has been effectively prevented and the binding between Aβ and Fe(III) is indeed strong.

Similar to our previous study of the Aβ−Cu(II) complex, the reduction potential of the Aβ−Fe(III)−NTA complex deduced from Figure 4 afforded an improved understanding of the redox species that can reduce the Aβ−Fe(III) complex in the cellular milieu. To reduce the Aβ−Fe(III)−NTA complex, a species must have a reduction potential more negative (higher reducing power) than 0.03 V versus Ag/AgCl or 0.23 V versus the normal hydrogen electrode (NHE). Since the Tyr-10 redox peak appears at ~0.78 V (*25*), we conclude that Tyr-10 cannot reduce the Aβ−Fe(III)−NTA complex. A Raman analysis of samples from deceased AD patients' brains indicated that Tyr-10 in Aβ was oxidized (*19*). Thus, one can reason that the Aβ−Cu(II) or Aβ−Fe(III) complex does not directly oxidize the Tyr-10 residue, and other cellular species or processes must be involved.

Similar to the electrochemistry of the Aβ−Cu(II) complex in solution (*25*), the Aβ−Fe(III)−NTA complex can be reduced to the Aβ−Fe(II)−NTA complex, once the cathodic scan has passed ~0.030 V:

$$A\beta\text{−Fe(III)−NTA}+e^- = A\beta\text{−Fe(II)−NTA} \quad (8)$$

The Aβ−Fe(II)−NTA complex or its analogue can subsequently react with O_2 in solution, producing H_2O_2:

$$2A\beta\text{−Fe(II)−NTA}+O_2+2H^+ = 2A\beta\text{−Fe(III)−NTA}+H_2O_2 \quad (9)$$

It is possible that eq 9 may have proceeded in a two-step reaction through the superoxide radical $O_2^{\bullet-}$, another important ROS:

$$A\beta\text{−Fe(II)−NTA}+O_2 = A\beta\text{−Fe(III)−NTA}+O_2^{\bullet-} \quad (10)$$

which subsequently reacts with protons on the Aβ molecule or a cellular species to produce H_2O_2:

$$O_2^{\bullet-}+2H^+ + A\beta\text{−Fe(II)−NTA} = A\beta\text{−Fe(III)−NTA}+H_2O_2 \quad (11)$$

$O_2^{\bullet-}$ is extremely reactive and cannot be detected voltammetrically. However, recent theoretical work by Hewitt and Rouk has shown that the mechanism described above, similar to the one that occurs to the superoxide dismutases in converting $O_2^{\bullet-}$ to H_2O_2 (*24*), is possible. Although the elucidation of the detailed mechanism in producing H_2O_2 and/or $O_2^{\bullet-}$ awaits further theoretical and experimental work, the measurement of the redox potential of a Fe(III)-containing Aβ species has provided vital information about the feasibility of these reactions.

The reactions described above are responsible for the O_2-dependent reduction peaks exhibited in Figure 4. As the potential of the Aβ−Fe(III)−NTA/Aβ−Fe(II)−NTA couple (0.23 V vs NHE) is lower than that of the O_2/H_2O_2 couple (0.295 V vs NHE) (*52*), eq 9 is thermodynamically allowed. We should point out that this study cannot rule out the possibility that some O_2 might be reduced to H_2O, via the reaction $O_2 + 4H^+ + 4e^- = 2H_2O$. However, on the basis of the amount of H_2O_2 detected, the reactions outlined above should constitute at least an important process.

From our spectrofluorometric measurements (Figure 5), it is clear that a prerequisite for H_2O_2 generation is the conversion of the Aβ−Fe(III)−NTA complex to the Aβ−Fe(II)−NTA complex. The amount of H_2O_2 generated must be dependent on all reactants [i.e., Aβ, Fe(III), and O_2]. Since in senile plaques the content of Aβ and the concentration of Fe(III) are both high and the function of brains requires a constant supply of O_2 (*53*), one would expect that the H_2O_2 concentration would be substantially high in AD brain. With regard to the biological relevance, it is interesting to note that mice do not develop AD (*54*) and their Aβ is different than the human variant at two of the potential metal binding sites, viz., His-13 and Tyr-10 (replaced with Arg and Phe, respectively). The decreased binding affinity toward metal ions may not inhibit the hydrolysis of Fe(III) to form redox-inactive iron oxide or hydroxide. In the case of familial AD, Aβ is point-mutated, but none of the mutations occurs in the metal binding region. These facts strongly suggest a possible role of iron binding by Aβ in producing H_2O_2 and other ROS to subsequently inflict oxidative stress in AD.

Given the relatively high reduction potential of the Aβ−Fe(III)−NTA/Aβ−Fe(II)−NTA couple (relatively high reducibility compared with that of the iron siderophore complex), a number of extracellular [e.g., ascorbic acid whose redox potential is 0.051 V vs NHE (*55*)], intracellular [e.g., glutathione whose redox potential is −0.228 V vs NHE (*38*)], and membrane species [e.g., the NADH dehydrogenase complex whose redox potential is −0.320 V vs NHE (*38*)] should be able to reduce the Aβ−Fe(III)−NTA complex or its analogue. A comprehensive list of biological reductants and their reduction potentials was provided in our previous paper (*25*). In addition to H_2O_2 generation and the multitude of deleterious consequences [e.g., production of hydroxyl radical through iron- or copper-facilitated "Fenton-like" reaction, and the subsequent damages of DNA, protein, and lipid molecules (*56*)], the catalytic nature of reactions shown in eqs 7 and 9 causes even a small amount of the Aβ−Fe(III) complex to cycle multiple times. Consequently, the levels of cellular antioxidants are diminished. Given the proximity of the redox potentials between the Aβ−Cu(II) and Aβ−Fe(III)−NTA complexes, the redox reactions that can be initiated by the Aβ−Cu(II) complex (*25*) are also applicable to those involving the Aβ−Fe(III)−NTA complex. We should point out that the iron content in brain [18.5 mg/100 g of wet tissue (*57*)] is greater than the quantity of copper [~0.5 mg/100 g of brain mass (*58*)]. It is therefore likely that iron contributes to metal-initiated oxidative stress in AD more than copper. In fact, the concentration of iron (0.9 mM) (*4*) is higher than that of copper (0.4 mM) (*4*) in senile plaques of AD patients, suggesting that both redox-active metals are involved and the extent of involvement is related to the overall metal loads in the brain.

A major characteristic of proteins that chaperone redox metal ions is their ability to significantly modulate redox potentials of the corresponding free metal ions. In terms of potentiating the redox potential of free Fe(III), Aβ, together with a small chelator (e.g., NTA), appears to possess such a property. In fact, it has been suggested that Aβ and its precursor, APP, might participate in sequestering and transporting metal ions (*21*). It has also been observed that cleavage of APP is dependent on the cellular iron content (*59*). However, the modulation of the redox activity of the Fe(III)/Fe(II) couple via Aβ complexation does not appear to be sufficient (from 0.77 to 0.23 V vs NHE) to completely prevent the complex from interacting with other biological redox species. Binding of iron by Aβ renders Fe(III) in a soluble form, and the Fe(III) center in a complex is still accessible to a range of cellular reductants. As a consequence, reactions such as those shown in eqs 7 and 9 or other redox processes can happen. This insufficient redox potentiation is in sharp contrast to that performed by other commonly known Fe-containing proteins. For example, the high content of iron stored by ferritin is in the redox-inactive oxide forms, and iron in transferrin has a redox potential of −0.40 V (vs NHE) (*60*), which is too negative (less reducible) for the Fe(III) center(s) to undergo electron transfer reactions with the aforementioned cellular reductants. Similarly, the iron center in hemoglobin is essentially redox inaccessible to many cellular reductants, and the redox potential of myoglobin is also mild [0.06 V vs NHE (*61*)]. By the same token, the primary requirement for an iron chelator used in chelation therapy for treating iron overload diseases (*62*) is that the resultant complex must possess a rather low (or negative) redox potential (low oxidizing power) to avoid toxicity that might arise from redox recycling of iron.

Another major difference between Aβ and transferrin is that the former has a much greater affinity for Fe(II). It is generally believed that the Fe(III) center(s) in transferrin is reduced to Fe(II) upon being internalized into cytosol. The binding affinity of transferrin for Fe(II) declines precipitously [by almost 17 orders of magnitude (*60*)], allowing Fe(II) to be sequestered by other cytosolic species. The rather strong binding of Aβ to Fe(II) (cf. Table 1) suggests that, even if Aβ (or APP) acts as a metal chaperone, its function and property are unconventional. Such a relatively strong binding, aided by a small chelator, withholds Fe(II) and disrupts the transport and homeostasis of iron. This might be at least part of the reason why iron coexists with Aβ aggregates in senile plaques. In addition, the Aβ−Fe(II) complex appears to be able to prevent the free Fe(II) from participating in the Fenton reaction to produce hydroxyl radical. A recent study by Baruch-Suchodolsky and Fischer showed that the Fe(II)-catalyzed generation of free radicals from H_2O_2 is halted by addition of Aβ (*16*). By measurement of dissociation constants of the complexes formed between Aβ and the Fe(III)−NTA or Fe(II)−NTA complex, insight into the role of Aβ in iron sequestration and the possible oxidative stress induced by iron can be gained. We note that the measured binding affinity (K_d = 6.3×10^{-21}) is close to those of transferrin (2.5×10^{-21} and 4.0×10^{-20} for the first and second irons, respectively) (*33*). Such a comparability implies that Aβ together with other small chelating

ligands can compete for Fe(III) from transferrin. The competition is particularly viable for Fe(III) bound in the c-lobe of transferrin (*33*). As a consequence, the iron content in these proteins will be decreased and their normal functions are altered. The upregulation of iron-responsive proteins (*63*) in AD brain may be associated with the loss of iron to Aβ. Equally detrimental is the accelerated aggregation of Aβ in the presence of metal ions. In short, sequestration of iron by Aβ sidetracks the normal homeostasis of iron and the proteolysis of Aβ.

Aβ may also accumulate iron from the labile iron pool. It is now commonly accepted that within the cytosol exists a transit labile iron pool in which iron is complexed by small organic chelators such as phosphates, citrates, carboxylates, polypeptides, and species at the membrane (e.g., phospholipid headgroups) (*21*, *34*). Iron in such a labile pool is transitory and will eventually become bound in metalloproteins. Thus, it is biologically relevant to study the properties of ternary complexes formed among Aβ, an organic chelator, and Fe(III) or Fe(II), since the small organic chelator not only provides additional stability to the transit iron but also further modulates the redox potential of the Fe(III)/Fe(II) couple. APP is known to be rapidly internalized into cytosol (*64*), within which complexation with iron in the labile iron pool and competitive replacement of iron in a metalloprotein can take place. Although at present it is not known whether iron complexation precedes or follows APP cleavage, the fact that Aβ can bind strongly to Fe(III) and Fe(II) to form redox-active complexes highlights the necessity of more extensive investigations of the properties of Aβ−Fe(III) or Aβ−Fe(II) complexes and their roles in triggering oxidative stress in AD.

CONCLUSIONS

We have, for the first time, observed the formation of ternary complexes among Aβ, NTA, and Fe(III) or Fe(II). The cumulative dissociation constants of the ternary complexes with Fe(III) and Fe(II) were determined to be 6.3×10^{-21} and 5.0×10^{-12} M^2, respectively. The binding affinity of Aβ for Fe(III) is comparable to that of transferrin, a strong iron-binding protein in brain, implying that Aβ together with a small chelator has the ability to compete for Fe(III) against a host of iron-containing proteins. Although Aβ binds to Fe(II) less strongly than to Fe(III), the affinity for Fe(II) is still considerably high (~8 orders of magnitude greater than that of transferrin!). Thus, Fe(II) converted from the Fe(III) center in the Aβ complex by cellular redox reactions is still withheld by Aβ. Using voltammetry, the redox potential of the complex was determined to be 0.03 V versus Ag/AgCl, representing a 0.54 V shift in the cathodic (negative) direction from the redox potential of the free Fe(III)/Fe(II) redox couple. Despite such a large modulation, the potentiation of the Fe(III) redox power by Aβ is still not adequate. As a result, the Fe(III) center can participate in a range of redox reactions. We have demonstrated that H_2O_2 can be generated by O_2 reduction catalyzed by the electrogenerated Aβ−Fe(II)−NTA complex. Taken together, the Aβ−Fe(III)−NTA/Aβ−Fe(II)−NTA couple behaves analogously to the well-studied Aβ−Cu(II)/Aβ−Cu(I) couple. Therefore, deleterious redox cycles of iron and copper could both occur in brain, facilitating the production of ROS and depleting essential cellular redox buffering species and antioxidants. The net outcome is that the complexation sidetracks the normal clearance of Aβ and the homeostasis of iron. The presence of the large quantities of iron and Aβ, as found in senile plaques, further exacerbates oxidative stress and accelerates the formation of other pernicious species such as the Aβ oligomers and fibrils.

SUPPORTING INFORMATION AVAILABLE

Extraction of the iron oxidation state from MS peaks of the Aβ(1−16)−Fe(III)−NTA adduct via ESI-MS of the +3 and +4 ions of the complex formed between Aβ(1−16) and the Fe(III)−NTA complex and MS^3 spectra contrasting the fragments generated from Aβ(1−16) and the Aβ(1−16)−Fe(III) complex. This material is available free of charge via the Internet at http://pubs.acs.org.

REFERENCES

1. Masters, C. L., Simms, G., Weinman, N. A., Multhaup, G., McDonald, B. L., and Beyreuther, K. (1985) Amyloid plaque core protein in Alzheimer disease and down syndrome. *Proc. Natl. Acad. Sci. U.S.A. 82*, 4245–4249.
2. Hardy, J. A., and Higgins, G. A. (1992) Alzheimer's disease: The amyloid cascade hypothesis. *Science 256*, 184–185.
3. Varadarajan, S., Yatin, S., Aksenova, M., and Butterfield, D. A. (2000) Review: Alzheimer's amyloid β-peptide-associated free radical oxidative stress and neurotoxicity. *J. Struct. Biol. 130*, 184–208.
4. Lovell, M. A., Robertson, J. D., Teesdale, W. J., Campbell, J. L., and Mardesbery, W. R. (1998) Copper, iron and zinc in Alzheimer's disease senile plaques. *J. Neurol. Sci. 158*, 47–52.
5. Smith, C. D., Carney, J. M., Starke-Reed, P. E., Oliver, C. N., Stadtman, E. R., Floyd, R. A., and Markesbery, W. R. (1991) Excess brain oxidation and enzyme dysfunction in normal aging and Alzheimer's disease. *Proc. Natl. Acad. Sci. U.S.A. 88*, 10540–10543.
6. Mecocci, P., MacGarvey, U., and Beal, M. F. (1994) Oxidative damage to mitochodrial DNA is increased in Alzheimer's disease. *Ann. Neurol. 36*, 747–751.
7. Markesbery, W. R., and Carney, J. M. (1999) Oxidative alterations in Alzheimer's disease. *Brain Pathol. 9*, 133–146.
8. Wang, Y. (2008) Bulky DNA lesions induced by reactive oxygen species. *Chem. Res. Toxicol. 21*, 276–281.
9. Svennerholm, L., and Gottfries, C. G. (1994) Membrane lipids, selectively diminished in Alzheimer's brains, suggest synapse loss as a primary event in early-onset and demyelination in late-onset form. *J. Neurochem. 62*, 1039–1047.
10. Hensley, K., Hall, N., Subramaniam, R., Cole, P., Harris, M., Aksenov, M., Aksenova, M., Gabbita, P., Wu, J. F., Carney, J. M., Lovell, M., Markesbery, W. R., and Butterfield, D. A. (1995) Brain regional correspondence between Alzheimer's disease histopathology and biomarkers of protein oxidation. *J. Neurochem. 65*, 2146–2156.
11. de la Monte, S. M., and Wands, J. R. (2006) Molecular indices of oxidative stress and mitochondrial dysfunction occur early and often progress with severity of Alzheimer's disease. *J. Alzheimer's Dis. 9*, 167–181.
12. Zhu, X., Smith, M. A., Perry, G., and Aliev, G. (2004) Mitochondrial failures in Alzheimer's disease. *Am. J. Alzheimer's Dis. Dementia 19*, 345–352.
13. Faller, P., and Hureau, C. (2009) Bioinorganic chemistry of copper and zinc ions coordinated to amyloid-β peptide. *Dalton Trans.*, 1080–1094.
14. Syme, C. D., Nadal, R. C., Rigby, S. E. J., and Viles, J. H. (2004) Copper binding to the amyloid-β peptide associated with Alzheimer's disease. *J. Biol. Chem. 279*, 18169–18177.
15. Shearer, J., and Szalai, V. A. (2008) The amyloid-β peptide of Alzheimer's disease binds CuI in a linear Bis-His coordination environment: Insight into a possible neuroprotective mechanism for the amyloid-β peptide. *J. Am. Chem. Soc. 130*, 17826–17835.
16. Baruch-Suchodolsky, R., and Fischer, B. (2008) Soluble amyloid-β(1−28) copper(I)/copper(II)/iron(II) complexes are potent antioxidants in cell-free systems. *Biochemistry 47*, 7796–7806.
17. Atwood, C. S., Scarpa, R. C., Huang, X., Moir, R. D., Jones, W. D., Fairlie, D. P., Tanzi, R. E., and Bush, A. I. (2000) Characterization of copper interactions with Alzheimer amyloid-β peptides: Identification of an attomolar-affinity copper binding site on amyloid β_{1-42}. *J. Neurochem. 75*, 1219–1233.
18. Kowalik-Jankowska, T., Ruta, M., Wisniewska, K., and Lankiewicz, L. (2003) Coordination abilities of the 1−16 and 1−28 fragments of β-amyloid peptide towards copper(II) ions: A combined potentiometric and spectroscopic study. *J. Inorg. Biochem. 95*, 270–282.

19. Dong, J., Atwood, C. S., Anderson, V. E., Siedlak, S. L., Smith, M. A., Perry, G., and Carey, P. R. (2003) Metal binding and oxidation of amyloid-β within isolated senile plaque cores: Raman microscopic evidence. *Biochemistry 42*, 2768–2773.
20. Evin, G. v., Zhu, A. Z., Holsinger, R. M. D., Masters, C. L., and Li, Q.-X. (2003) Proteolytic processing of the Alzheimer's disease amyloid precursor protein in brain and platelets. *J. Neurosci. Res. 74*, 386–392.
21. Sigel, A., Sigel, H., and Sigel, R. K. O. (2006) Metal ions in life sciences, Vol. 1, John Wiley & Sons, West Sussex, U.K.
22. Bayer, T. A., and Multhaup, G. (2005) Involvement of amyloid β precursor protein (AβPP) modulated copper homeostasis in Alzheimer's disease. *J. Alzheimer's Dis. 8*, 1387–2877.
23. Huang, X., Cuajungco, M. P., Atwood, C. S., Hartshorn, M. A., Tyntall, J. D. A., Hanson, G. R., Stokes, K. C., Leopold, M., Multhaup, G., Goldstein, L. E., Scarpa, R. C., Saunders, A. J., Lim, J., Moir, R. D., Glabe, C., Bowden, E. F., Masters, C. L., Fairlie, D. P., Tanzi, R. E., and Bush, A. (1999) Cu(II) potentiation of Alzheimer's Aβ neurotoxicity. *J. Biol. Chem. 274*, 37111–37116.
24. Hewitt, N., and Rauk, A. (2009) Mechanism of hydrogen peroxide production by copper-bound amyloid β peptide: A theoretical study. *J. Phys. Chem. B 113*, 1202–1209.
25. Jiang, D., Men, L., Wang, J., Zhang, Y., Chickenyen, S., Wang, Y., and Zhou, F. (2007) Redox reactions of copper complexes formed with different β-amyloid peptides and their neuropathalogical relevance. *Biochemistry 46*, 9270–9282.
26. Wallander, M. L., Leibold, E. A., and Eisenstein, R. S. (2006) Molecular control of vertebrate iron homeostasis by iron regulatory proteins. *Biochim. Biophys. Acta 1763*, 668–689.
27. Kuiper, M. A., Mulder, C., van Kamp, G. J., Scheltens, P., and Wolters, E. C. (1994) Cerebrospinal fluid ferritin levels of patients with Parkinson's disease, Alzheimer's disease, and multiple system atrophy. *J. Neural. Transm. 7*, 109–114.
28. Morgan, C., Colombres, M., Nunez, M. T., and Inestrosa, N. C. (2004) Structure and function of amyloid in Alzheimer's disease. *Prog. Neurobiol. 74*, 323–349.
29. Sayre, L. M., Perry, G., Harris, P. L. R., Liu, Y., Schubert, K. A., and Smith, M. A. (2000) In situ oxidative catalysis by neurofibrillary tangles and senile plaques in Alzheimer's disease. *J. Neurochem. 74*, 270–279.
30. Smith, M. A., Harris, P. L. R., Sayre, L. M., and Perry, G. (1997) Iron accumulation in Alzheimer disease is a source of redox-generated free radicals. *Proc. Natl. Acad. Sci. U.S.A. 94*, 9866–9868.
31. Rae, T. D., Schmidt, P. J., Pufahl, R. A., Culotta, V. C., and O'Halloran, T. V. (1999) Undetectable free intracellular copper: The requirement of a copper chaperone for superoxide dismutase. *Science 284*, 805–808.
32. Schlabach, M. R., and Bates, G. W. (1975) The synergistic binding of anions and Fe^{3+} by transferrin. *J. Biol. Chem. 250*, 2182–2188.
33. Aisen, P., Leibman, A., and Zweiser, J. (1978) Stoichiometric and site characteristics of the binding of iron to human transferrin. *J. Biol. Chem. 253*, 1930–1937.
34. Kakhlon, O., and Cabantchik, Z. I. (2002) The labile iron pool: Characterization, measurement, and participation in cellular processes. *Free Radical Biol. Med. 33*, 1037–1046.
35. Mwanjewe, J., Hui, B. K., Coughlin, M. D., and Grover, A. K. (2001) Treatment of PC12 cells with nerve growth factor increases iron uptake. *Biochem. J. 357*, 881–886.
36. Demmink, J. F., and Beenackers, A. A. C. M. (1997) Oxidation of ferrous nitrilotriacetic acid with oxygen: A model for oxygen mass transfer parallel to reaction kinetics. *Ind. Eng. Chem. Res. 36*, 1989–2005.
37. Maitti, N. C., Jiang, D., Wain, A. J., Patel, S., Dinh, K. L., and Zhou, F. (2008) Mechanistic studies of Cu(II) binding to amyloid-β peptides and fluorescence and redox behaviors of the resulting complexes. *J. Phys. Chem. B 112*, 8406–8411.
38. Dryhurst, G., Kadish, K. M., Scheller, F., and Renneberg, R. (1982) Biological Electrochemistry , Vol. 1, Academic Press, New York.
39. Curtain, C. C., Ali, F., Volitakisi, I., Chernyi, R. A., Norton, R. S., Beyreuther, K., Barrow, C. J., Mastersi, C. L., Bush, A. I., and Barnham, K. J. (2001) Alzheimer's disease amyloid-β binds copper and zinc to generate an allosterically ordered membrane-penetrating structure containing superoxide dismutase-like subunits. *J. Biol. Chem. 276*, 20466–20473.
40. Varadarajan, S., Kanski, J., Aksenova, M., Lauderback, C., and Butterfield, D. A. (2001) Different mechanisms of oxidative stress and neurotoxicity for Alzheimers Aβ(1−42) and Aβ(25−35). *J. Am. Chem. Soc. 123*, 5625–5631.
41. Schoneich, C., Pogocki, D., Hug, G. L., and Bobrowski, K. (2003) Free radical reactions of methionine in peptides: Mechanisms relevant to β-amyloid oxidation and Alzheimer's disease. *J. Am. Chem. Soc. 125*, 13700–13713.
42. Sanaullah, Wilson, G. S., and Glass, R. S. (1994) The effect of pH and complexation of amino acid functionality on the redox chemistry of methionine and X-ray structure of $[Co(en)_2(L\text{-}Met)](ClO_4)_2 \cdot H_2O$. *J. Inorg. Biochem. 55*, 87–99.
43. Cooper, S. R., Mcardle, J. V., and Raymond, K. N. (1978) Siderophore electrochemistry: Relation to intracellular iron release mechanism. *Proc. Natl. Acad. Sci. U.S.A. 75*, 3551–3554.
44. Bard, A. J., and Faulkner, L. R. (2000) Electrochemical methods: Fundamentals and applications , 2nd ed., John Wiley & Sons, New York.
45. Weast, R. C. (1970) CRC Handbook of Chemistry and Physics , 51st ed., The Chemical Rubber Co., Cleveland, OH.
46. Garzon-Rodriguez, W., Yatsimirsky, A. K., and Glabe, C. G. (1999) Binding of Zn(II), Cu(II), and Fe(II) ions to Alzheimer's all peptide studied by fluorescence. *Bioorg. Med. Chem. Lett. 9*, 2243–2248.
47. Chahine, J.-M., and Fain, D. (1993) The mechanism of iron transferrin interactions. Uptake of the iron nitrilotriacetic acid complex. *J. Chem. Soc., Dalton Trans.,* 3137–3143.
48. Khan, A., Dobson, J. P., and Exley, C. (2006) Redox cycling of iron by $A\beta_{42}$. *Free Radical Biol. Med. 40*, 557–569.
49. McCreery, R. L., and Cline, C. K. (1996) Carbon electrodes. In Laboratory Techniques in Electroanalytical Chemistry (Kissinger, P. T., and Heineman, W. R., Eds.) p 293, Marcel Dekker, Inc., New York.
50. Karr, J. W., Akintoye, H., Kaupp, L. J., and Szalai, V. A. (2005) N-Terminal deletions modify the Cu^{2+} binding site in amyloid-β. *Biochemistry 44*, 5478–5487.
51. Karr, J. W., Kaupp, L. J., and Szalai, V. A. (2004) Amyloid-β binds Cu^{2+} in a mononuclear metal ion binding site. *J. Am. Chem. Soc. 126*, 13534–13538.
52. Lehninger, A. L., Nelson, D. L., and Cox, M. M. (2004) Principles of Biochemistry , 4th ed., W. H. Freeman & Co., New York.
53. Kandel, E. R., Schwartz, J. H., and Jessell, T. M. (2000) Principles of Neural Science , McGraw-Hill, New York.
54. Vaughan, D. W., and Peters, A. (1981) The structure of neuritic plaque in cerebral cortex of aged rats. *J. Neuropathol. Exp. Neurol. 40*, 472–487.
55. Conway, B. E. (1969) Electrochemical Data, Greenwood Press, Westport, CT.
56. Cao, H., and Wang, Y. (2007) Quantification of oxidative single-base and intrastrand cross-link lesions in unmethylated and CpG-methylated DNA induced by Fenton-type reagents. *Nucleic Acids Res. 35*, 4833–4844.
57. Arreguin, S., Nelson, P., Padway, S., Shirazi, M., and Pierpont, C. (2009) Dopamine complexes of iron in the etiology and pathogenesis of Parkinson's disease. *J. Inorg. Biochem. 103*, 87–93.
58. Macreadie, I. G. (2008) Copper transport and Alzheimer's disease. *Eur. Biophys. J. 37*, 295–300.
59. Bodovitz, S., Falduto, M. T., Frail, D. E., and Klein, W. L. (2002) Iron levels modulate α-secretase cleavage of amyloid precursor protein. *J. Neurochem. 64*, 307–315.
60. Harris, W. R. (1986) Estimation of the ferrous-transferrin binding constants based on thermodynamic studies of nickel(II)-transferrinH. *J. Inorg. Chem. 27*, 41–52.
61. Takashi, M., Hirohisa, D., Shun, H., Dai, M., Hideaki, S., Takahiro, I., Hiroshi, H., Yoshio, H., and Takashi, H. (2004) Ligand binding properties of myoglobin reconstituted with iron porphyrin: Unusual O_2 binding selectivity against CO binding. *J. Am. Chem. Soc. 126*, 16007–16017.
62. Hider, R. C., and Zhou, T. (2006) The design of orally active iron chelators. *Ann. N.Y. Acad. Sci. 1054*, 141–154.
63. Zhu, X., Raina, A. K., Lee, H.-G., Casadesus, G., Smith, M. A., and Perry, G. (2004) Oxidative stress signaling in Alzheimer's disease. *Brain Res. 1000*, 32–39.
64. Sisodia, S. S., and Tanzi, R. E. (2007) Alzheimer's Disease, Advances in Genetics, Molecular and Cellular Biology , Springer Science, New York.